Article

Photocorrosion Inhibition and Photoactivity Enhancement for Zinc Oxide via Hybridization with Monolayer Polyaniline

Hao Zhang, Ruilong Zong, and Yongfa Zhu

J. Phys. Chem. C, **2009**, 113 (11), 4605-4611• DOI: 10.1021/jp810748u • Publication Date (Web): 18 February 2009

Photocorrosion Inhibition and Photoactivity Enhancement for Zinc Oxide via Hybridization with Monolayer Polyaniline

Hao Zhang, Ruilong Zong, and Yongfa Zhu*

Department of Chemistry, Tsinghua University, Beijing 100084, PR China

Received: December 7, 2008; Revised Manuscript Received: January 17, 2009

Monomolecular-layer polyaniline (PANI) was dispersed on the surface of zinc oxide (ZnO) and formed the hybrid effect between ZnO and PANI. The hybrid photocatalysts showed dramatic photocatalytic activity for the degradation of the methylene blue (MB) both under ultraviolet and visible light irradiation, and the photocorrosion of ZnO was successfully inhibited. The enhanced photocatalytic activity for PANI-hybridized ZnO originated from the high separation efficiency of photogenerated electrons and holes on the interface of PANI and ZnO, which was produced by the hybrid effect of PANI and ZnO. The photocorrosion inhibition of ZnO could be attributed to the rapidly transferring of photogenerated holes by the PANI monolayer. The relationship between the PANI content of the samples and their photocatalytic performance shows that an optimal PANI weight percent (1.0%) can significantly enhance the photocatalytic efficiency and anticorrosion of ZnO particles. In particular, the mechanisms on the enhancement of photocatalytic activity and antiphotocorrosion performance have been emphasized. Under ultraviolet light irradiation, photogenerated holes in the ZnO valence band could transfer to the HOMO orbital of PANI and then emigrate to the photocatalysts surface and oxidize the adsorbed contaminants directly. Under visible light irradiation, PANI generated a $\pi^{-}\pi^{*}$ transition, delivering the excited electrons to the conduction band of ZnO, and then the electrons transferred to an adsorbed electron acceptor, yielding oxygenous radicals to degrade pollutants.

1. Introduction

Semiconductor-assisted photocatalysis has attracted considerable attention as a promising tool for implementing the purification of wastewater and hydrogen energy production.[1−4] Among various semiconducting materials, although TiO_2 is extensively investigated and widely employed,[5,6] some studies have highlighted that ZnO exhibits better efficiency than TiO_2 for removing organic compounds in water matrices and photoelectric conversion.[7−10] Unfortunately, because of its quick recombination of charge carriers, very poor response to visible light, and critical drawback of photocorrosion, ZnO cannot be utilized for direct solar illumination, and the photoactivity and photostability are significantly reduced.[11,12] This fundamental disadvantage has remained a major obstacle in its performance in environmental mediation and solar conversion. Thus, significant effort has been devoted to reducing the recombination of photogenerated hole−electron pairs and enhancing the absorption of solar light irradiation during the photocatalytic reactions by surface modification,[13−21] such as depositing metals on ZnO surface,[13−16] or doping with metals or metal ions,[17,18] or combining ZnO with another semiconductor.[19−21]

Recently, materials with delocalized conjugated structures have been extensively studied for their rapid photoinduced charge separation and a relatively slow charge recombination in electron-transfer processes.[22−26] PANI by itself is known to be an efficient conductive polymer with variety of unique properties.[27] It has been reported that PANI contains an extensively conjugated π system and is also regarded as a fine photogenerated hole-transporting material,[28,29] which is suitable for efficient electron and hole transfer. In a previous paper, we demonstrated that the presence of PANI monolayer molecules on an oxide surface can affect the photocatalytic activity of TiO_2 nanocrystals remarkably.[25] The present work further explores this topic by considering the case of zinc oxide. Judging from the excellent photocatalyst of ZnO and the efficient carrier transfer property of PANI, the combination of ZnO and PANI seems to be ideal for fulfilling enhanced photon efficiency and suppressing photocorrosion. It is expected that coating the surface of ZnO with a preferred PANI material will enable us to construct a PANI-based ZnO catalyst, not only to obtain higher efficiency but also to avoid the photocorrosion of ZnO.

Herein, we present the first example of PANI monolayer−hybrid ZnO fabricated by the chemisorption method that demonstrates that a hybrid effect exists between ZnO and PANI, which causes the high separation efficiency of photogenerated electron−hole pairs. This hybrid effect resulting in the photocorrosion of ZnO was completely suppressed and generated dramatic visible photoactivity. The possible mechanisms of photocorrosion inhibition and enhancement of photocatalytic activity via hybridization have been established in detail. It is anticipated that this model hybrid photocatalyst will enable us to design high-activity, high-stability, visible-light-driven photocatalysts in the future.

2. Experimental Section

2.1. Materials Preparation. PANI (molecular weight $\sim 10^5$) was purchased from Jilin Zhengji Corp (PR China). ZnO (particle diameter 20 nm, surface area 21.5 $m^2 \cdot g^{-1}$) was obtained from Nanjing Haitai Nanometer Materials Corp (PR China). All chemicals were reagent grade and were used without further purification. A PANI-hybridized ZnO sample was prepared as follows: an amount of ZnO powder was added to 100 mL of 0.45 $g \cdot L^{-1}$ PANI (THF) solution, sonicated for 30 min to ensure that the ZnO sample was totally dispersed, and then stirred for 24 h. The suspension was filtered, and the precipitate was

* Corresponding author. E-mail: zhuyf@tsinghua.edu.cn.

10.1021/jp810748u CCC: $40.75
Published on Web 02/18/2009

washed with water three times and transferred to an oven to dry at 60 °C for 24 h. PANI-hybridized ZnO samples with different mass ratios from 0.5 to 3.0% were prepared by following the same procedure as above. To test the photoelectrochemical performance of a PANI-hybridized ZnO sample, the sample dispersed in ethanol solution was evenly spread onto ITO (indium tin oxide) glass substrates (3 cm × 2 cm) with a sheet resistance of 15 Ω. After being dried, the as-prepared electrodes were dried at 100 °C for 24 h.

2.2. Characterization. XRD patterns of the powders were recorded on a Bruker D8 Advance XRD diffractometer with Cu Kα radiation. Diffusion reflection spectra (DRS) collection was carried out on a Hitachi U-3010 instrument with $BaSO_4$ as the reference sample. The Brunauer−Emmett−Teller (BET) surface area measurements were performed by a Micromeritics (ASAP2010 V5.02H) surface area analyzer. FTIR spectra were recorded by using a Perkin-Elmer System 2000 infrared spectrometer with KBr as the reference sample. Raman spectra (LRS) were recorded on an RM 2000 microscopic confocal Raman spectrometer (Renishaw Company) with excitation by 633 nm laser light. Transmission electron microscopy (TEM) and high-resolution transmission electron microscopy (HRTEM) images were obtained on a JEM2010 transmission electron microscope operated at accelerating voltages of 120 and 200 kV, respectively. The photoelectrochemical experiment was carried out on an electrochemical system (CHI-660B, China).

2.3. Photocatalytic Experiments. The photocatalytic activities were evaluated by the decomposition of MB under UV light ($\lambda = 254$ nm) and visible light ($\lambda > 450$ nm), respectively. The UV light was obtained via an 11 W germicidal lamp (Institute for Electric Light Sources, Beijing), and the average light intensity was 1.8 mW·cm^{-2} as measured by a power meter from the Institute for Electric Light Sources, Beijing. Aqueous suspensions of MB (100 mL, 15 mg·L^{-1}) were placed in a vessel, and 50 mg of photocatalysts was added. Prior to irradiation, the suspensions were magnetically stirred in the dark for about 30 min. The suspensions were kept under constant air-equilibrated conditions before and during illumination. At certain time intervals, 2 mL aliquots were sampled and centrifuged to remove particles. The filtrates were analyzed by recording variations in the maximum absorption band (633 nm) using a Hitachi U-3010 UV−vis spectrophotometer. The visible light was obtained by a 500 W xenon lamp (Institute for Electric Light Sources, Beijing) with a 450 nm cutoff filter to ensure the desired irradiation light and that the average light intensity was 44.5 mW· cm^{-2}. The method was similar to a UV light test. The active oxidants generated in the photocatalytic process could be measured through trapping by tert-butyl alcohol (*t*BuOH) and disodium ethylenediamine tetraacetate (EDTA-2Na).

2.4. Photoelectrochemical Measurements. Photoelectrochemical tests were carried out in a conventional three-electrode, single-compartment quartz cell, filled with 0.1 M Na_2SO_4 electrolyte (130 mL), using a potentiostat. The ITO/ZnO or ITO/PANI-ZnO electrode served as the working electrode. The counter and reference electrodes were a platinum black plate and a saturated calomel electrode (SCE), respectively. An 11 W germicidal lamp and a 500 W xenon lamp were used as the excitation light sources for UV and visible irradiation, respectively. Electrochemical impedance spectra (EIS) were recorded in potentiostatic mode. The amplitude of the sinusoidal wave was 10 mV, and the frequency range of the sinusoidal wave was from 100 kHz to 0.05 Hz. For maximum incident photon-to-electron conversion efficiency (IPCE) measurements, a solution of 0.05 M I_2 and 0.5 M LiI in propylene carbonate was used as an electrolyte. The monochromatic light was from a 500 W xenon lamp, which was passed through a SAP301 grating monochromator (Zolix Instruments Co., Ltd., Beijing), and the wavelength was selected at 10 nm intervals between 300 and 560 nm.

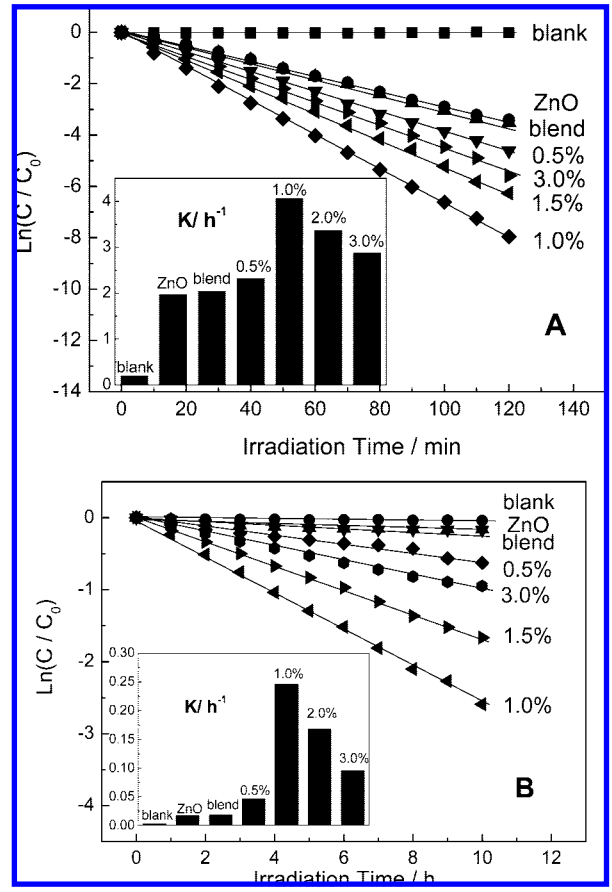

Figure 1. Photocatalytic degradation of MB over the as-prepared samples (A) under ultraviolet light irradiation and (B) under visible light irradiation ($\lambda > 450$ nm); catalyst loading, 0.5 g·L^{-1}; MB, 1.5 × 10^{-5} M. (Inset) Rate constant *k* as a function of PANI content.

3. Results and Discussions

3.1. Enhancement of Photocatalytic Activity. Figure 1 shows the photocatalytic activity of ZnO and the various PANI-hybridized ZnO samples as a plot of the degradation of MB under ultraviolet and visible light irradiation, respectively. As a photocatalytic reference, mechanically blended PANI and ZnO (1:100 w/w) were used to evaluate the photoactivity qualitatively. Significant differences in the catalytic behaviors were observed, and the photodegradation process was fit to pseudo-first-order kinetics in which the value of rate constant *k* is equal to the corresponding slope of the fitting line. Under UV light irradiation (Figure 1A), the absence of a catalyst and the blended samples of PANI and ZnO had no notable effect on the degradation of MB, whereas all of the hybridized ZnO samples exhibited higher photocatalytic activity than did the pure ZnO sample. The sample with 1.0% PANI had the highest activity, which was increased about 2-fold compared to that for the ZnO sample. It also could be seen from the inset graph of Figure 1A that the loading amount of PANI had a great influence on the photocatalytic activity of the as-prepared samples and as the PANI content increased, the photocatalytic performance of the PANI−ZnO nanoparticles did not enhance monotonously. When

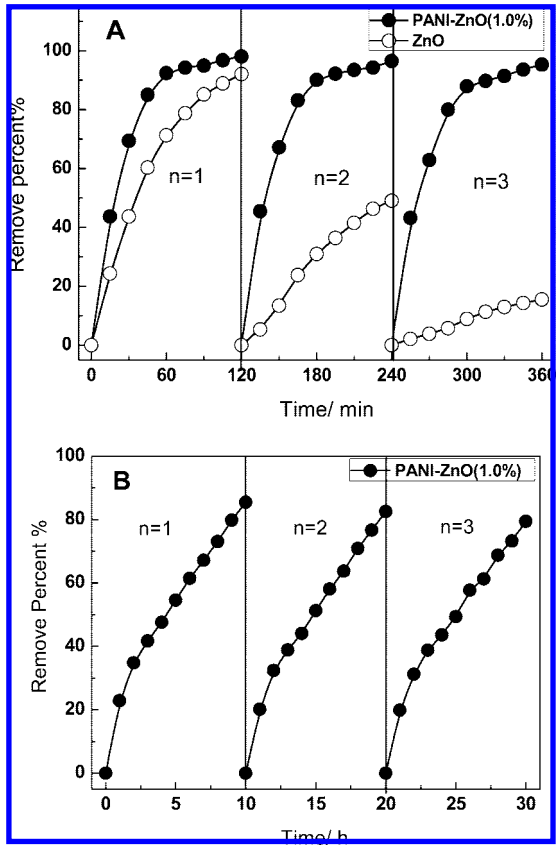

Figure 2. Plots of the percentage of MB removed during photocatalytic recycle degradation as a function of the irradiation period: (A) under ultraviolet light irradiation and (B) under visible light irradiation ($\lambda >$ 450 nm).

the PANI content was relatively low (<1.0%), the photocatalytic activity of PANI−ZnO increased continuously. Alternatively, when the PANI content is relatively high (>1.0%), the photocatalytic activity of PANI−ZnO decreased with increasing PANI content. Thus, the optimal PANI content was approximately 1.0%, to which 98% MB could be degraded in 10 h. Under visible light irradiation ($\lambda >$ 450 nm), the pure ZnO photocatalysts played no role in removing MB because ZnO is not excited by visible light irradiation. All of the hybridized ZnO samples possessed excellent visible light photocatalytic activity. The influence of PANI content upon the visible light photocatalytic activity was shown in the inset graph of Figure 1B, which was similar to that of UV photoactivity. At PANI content higher than the optimized content (1.0%), the PANI molecules accumulated on a ZnO surface may encourage the recombination of charge carriers and reduce the availability of pollutant adsorption, which decreases the photocatalytic efficiency of the semiconductor. It is notable that the mechanical blend evidently did not enhance the photocatalytic activity, which implies that there may be some interaction between ZnO and PANI that plays a crucial role in improving the photocatalytic activity of the ZnO semiconductor.

3.2. Inhibition of ZnO Photocorrosion. To evaluate the photostability of the catalyst, recycled experiments for the photodegradation of MB were performed, and the results are shown in Figure 2. Under UV light irradiation, 92% of MB could be degraded within 120 min when ZnO was used for the first time; however, after three recycles, a significant decrease in photocatalytic activity for pure ZnO was found in which only 16% of MB was degraded (Figure 2A). The drastic decrease in photocatalytic activity for ZnO resulted from the photocorrosion effect.[11,12] After the ZnO photocatalyst was hybridized by PANI, the recycled use of PANI−ZnO (1.0%) three times did not conspicuously affect its photocatalytic activity. Apparently, the photocorrosion effect of ZnO was inhibited by PANI molecules after hybridization. Under visible light irradiation (Figure 2B), 86% of MB could be degraded over PANI−ZnO (1.0%) within 10 h when used for the first time, and the samples presented continuously stable visible light photocatalytic activity during the recycled reaction. In this system, the presence of hybridized PANI on the surface of ZnO suppressed the photocorrosion phenomenon and enhanced the stability of the catalyst greatly both under UV and visible light irradiation.

The inhibition of photocorrosion can be further investigated by XRD patterns and TEM images before and after photocatalytic reaction for three recycles. The reaction products were treated without further washing to ensure that no components were lost. In XRD patterns (Figure 3), it could be found that PANI−ZnO (1.0%) had a crystalline phase structure similar to that of ZnO and no peaks assigned to PANI were observed because the PANI layer was too thin. For pure ZnO, after the photocatalytic recycle reaction, the crystalline phase structure was destroyed disastrously, which indicated that severe photocorrosion had taken placed. The XRD patterns of PANI-ZnO (1.0%) had no notable differences before and after the photocatalytic recycles under both UV and visible light irradiation. In TEM experiments (Figure S1, Supporting Information), ZnO and PANI−ZnO samples consisted of agglomerated approximately spherical particles with diameters of 10−20 nm. For PANI−ZnO (1.0%) before and after photocatalytic recycles under UV and visible irradiation, respectively, it had not exhibited any great loss in morphology, revealing that PANI-hybridized ZnO was photostable and not photocorroded. As for pure ZnO, after the photocatalytic recycles, the spherical particles disappeared, and only weblike morphologies existed, indicating that the structure of the ZnO crystal had already been demolished. The TEM result was in reasonable agreement with the results of XRD tests, further indicating that the photocorrosion effect of ZnO was successfully inhibited by hybridized PANI molecular on its surface. Moreover, we show that such a small amount of hybridized PANI can be easily stabilized and hardly decomposed, ensuring that there was no secondary pollution and thus for practical reasons ensuring a long lifetime for this modified ZnO photocatalyst.

3.3. Hybrid Structures. It was well known that the photocatalytic activity is governed by various factors such as surface area, phase structure, interfacial charge transfer, and separation efficiency of photogenerated electrons and holes.[5] The XRD patterns of various pure PANI-hybridized ZnO nanoparticles (Figure S2, Supporting Information) indicated that the crystallinity of the samples did not change very much. The content of PANI might be too small to determine its existence, which possibly indicates that PANI is dispersed uniformly onto the surfaces of ZnO nanoparticles.[26] The diffuse reflectance absorption spectra (Figure S3, Supporting Information) illustrate that compared with the pure ZnO, PANI-hybridized ZnO showed almost the same absorbance edge but extended the absorbance to the visible region as far as 800 nm. The specific surface area, evaluated by the BET equation from nitrogen adsorption isotherms at 77 K, indicates there was no appreciable change in the surface area before (21.5 $m^2\ g^{-1}$) and after hybridization (20.1 $m^2\ g^{-1}$). Because the surface area and phase structure of ZnO remained almost the same before and after being modified by PANI, we may conclude that the separation of the photogenerated electrons and holes plays an important part in the

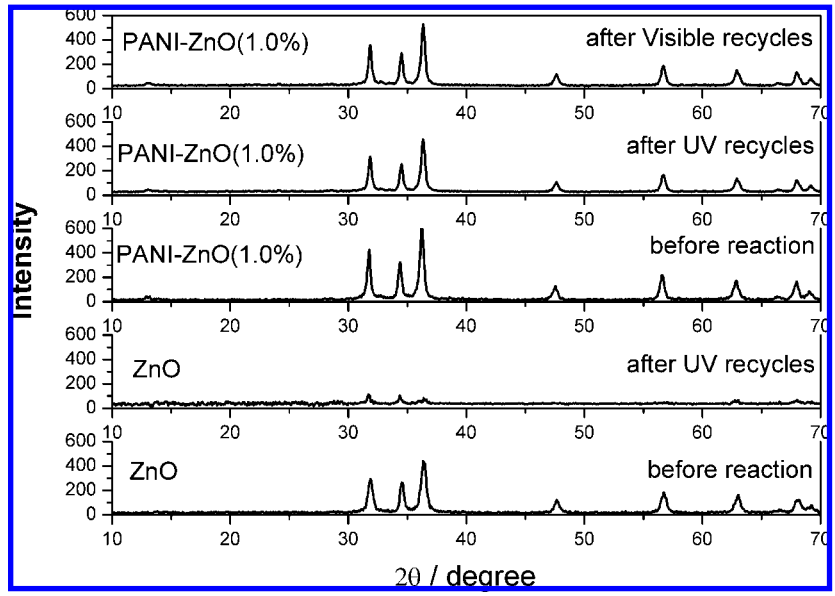

Figure 3. Plots of XRD patterns of ZnO and PANI−ZnO (1.0%) before and after the photocatalytic degradation of MB for three recycles, under UV and visible light irradiation ($\lambda > 450$ nm), respectively.

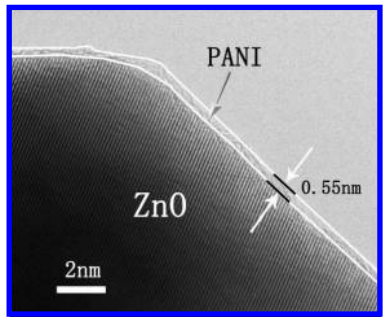

Figure 4. HRTEM images of PANI−ZnO (1.0%).

enhancement of the photocatalytic activity of the hybrid photocatalysts. Considering that the diameter of benzene was about 0.5 nm[25] and the BET surface area of ZnO was 21.5 m^2 g^{-1}, it was estimated that the weight ratio at which nearly compact PANI monolayer coverage was formed on the surface of ZnO was about 1.3%;[25] the actual ratio of PANI absorbed on the surface of ZnO could be less than 1.3% because PANI can occupy only the active absorption site on the surface of ZnO.[26]

The high separation efficiency of photogenerated carriers is mainly related to the interface structure of PANI−ZnO photocatalysts. The typical morphologies of the as-prepared PANI−ZnO sample (1.0%) were observed using HRTEM (Figure 4). It was found that the lattice structure of ZnO was very orderly and the outer boundary of the as-prepared sample was distinctly different from the ZnO core. It revealed clearly that the PANI layer with noncrystal structure adsorbed evenly and stably on the ZnO surface with the thickness of about 0.5−0.6 nm. The PANI molecule has a fold-line frame structure, and the diameter of the benzene structure is about 0.5 nm, which is close to the scale of monolayer PANI.[25] Therefore, it can be speculated that the PANI molecule was dispersed on the surface of ZnO with monolayer structure. This estimation is based on the assumption that each PANI molecule occupies approximately 100% and is spread evenly on the ZnO surface.[26]

To obtain information on the structure of the PANI−ZnO complex, its Raman and FTIR spectra were studied (Figure 5). In the representative Raman spectra of PANI (Figure 5A), the

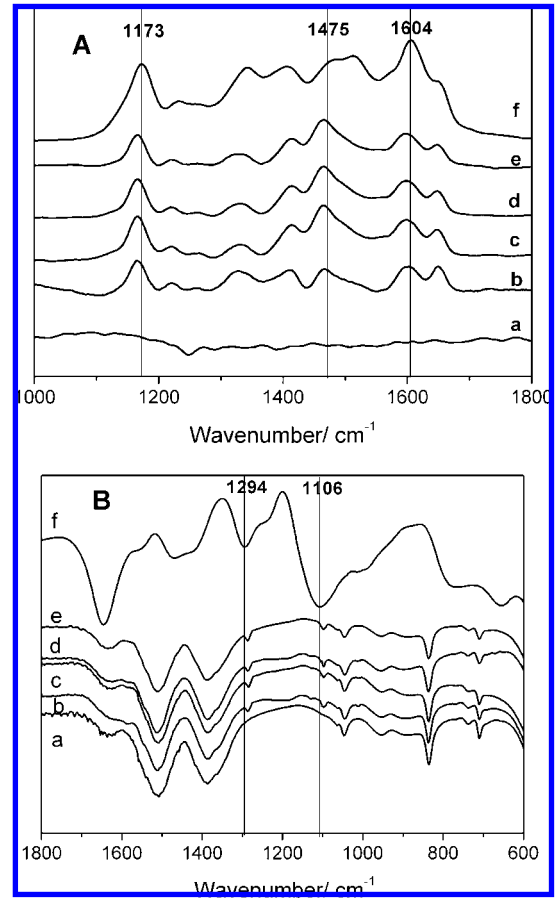

Figure 5. (A) LRS spectra of ZnO and various PANI−ZnO photocatalysts. (B) FTIR spectra of ZnO and various PANI−ZnO photocatalysts: (a) ZnO, (b) PANI−ZnO (0.5%), (c) PANI−ZnO (1.0%), (d) PANI−ZnO (2.0%), (e) PANI−ZnO (3.0%), and (f) PANI.

bands around 1605 cm^{-1} were attributable to the benzenoid unit vibrational mode. A peak near 1476 cm^{-1} was assigned to the quinonoid unit vibrational mode, and the peak at about 1173 cm^{-1} was the C−H bending mode.[30] In the PANI−ZnO composite, all of these bands moved to lower wavenumber. The red shift of these bands suggested that the bond strengths of

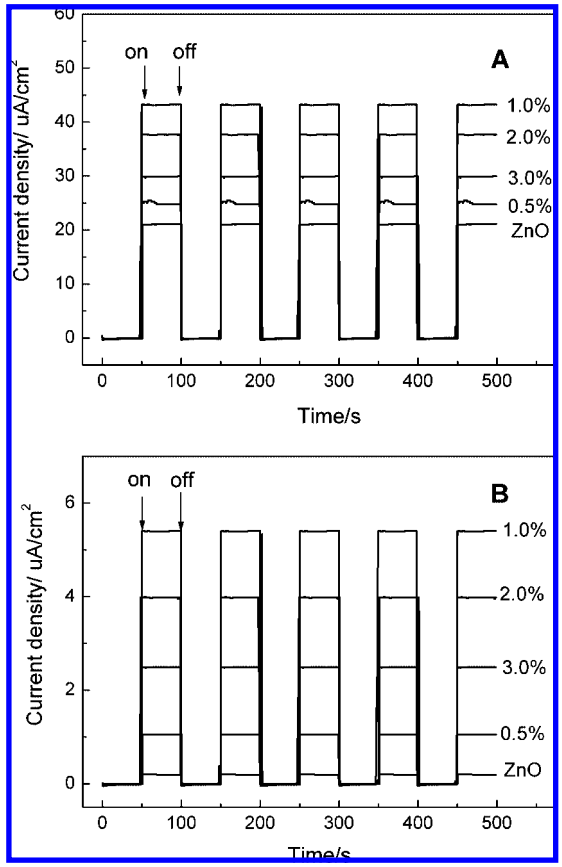

Figure 6. Photocurrent spectra of ITO/ZnO and various ITO/PANI−ZnO electrodes (A) under ultraviolet light irradiation and (B) under visible light irradiation ($\lambda > 450$ nm).

C═N (C═C) and C−N were weakened so that the PANI conjugated bond was stretched and a more widely conjugated chain containing PANI and ZnO had already appeared. It can be inferred that an intense interaction existed between PANI and ZnO. This interaction can be further revealed by infrared spectroscopy. The FTIR spectra of ZnO, PANI, and various PANI-hybridized ZnO photocatalysts are shown in Figure 5B. The hybridization between ZnO and PANI molecules resulted in some changes in the FTIR spectrum of PANI. In the IR spectra of PANI−ZnO, the peaks of pure PANI at 1560 cm^{-1} (C═N and C═C stretching modes) and 1294 cm^{-1} (C−N stretching mode)[30,31] shifted to lower wavenumber, indicating that all of these chemical bonds were weakened. According to the results of Raman and FTIR, the hybridization between ZnO and PANI molecules resulted in an intense interaction and the chemical-adsorbed monolayer PANI structure caused an interface hybrid effect between PANI and ZnO.[25,26]

On the basis of all of the above results, it could be concluded that the PANI molecule was bonded on the surface of ZnO, forming a monomolecular layer, and there existed an intimate hybrid effect between PANI and the ZnO phase. This hybrid effect was essential to promoting the separation efficiency of photogenerated carriers and enhancing photocatalytic activity and antiphotocorrosion performance.

3.4. Enhancement of Interface Charge Separation Efficiency. The interface charge separation efficiency can be investigated by all kinds of photoelectrochemical tests, such as photocurrent spectra, electrochemical impedance spectroscopy (EIS), and maximum incident photon-to-electron conversion efficiency (IPCE). In Figure 6A, the photocurrent under UV irradiation was enhanced after hybridization by PANI, and with

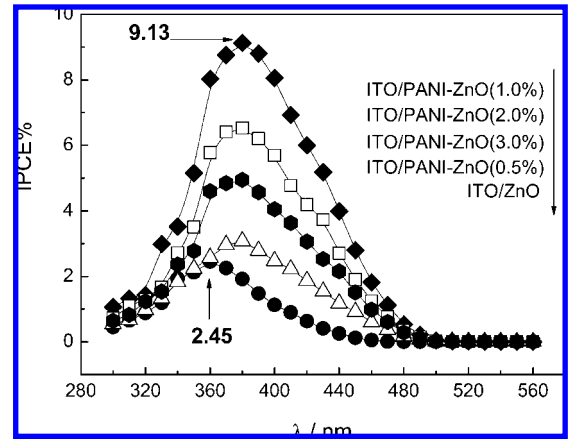

Figure 7. Photocurrent action spectra of ITO/ZnO and various ITO/PANI−ZnO electrodes.

the amount of PANI increasing, the photocurrent of the ITO/PANI−ZnO electrode that was revealed first increased and then decreased though it was much larger than that of the ITO/ZnO electrode all along. The ITO/PANI−ZnO (1.0%) electrode had the largest photocurrent, which was about 2.1 times compared with that of an ITO/ZnO electrode. In Figure 6B, under visible irradiation, the photocurrent had dramatically increased after hybridization and presented a similar change trend to that of UV irradiation. Also, the maximum photocurrent appeared at a weight ratio of 1.0%. EIS was used to investigate the photogenerated charge separation process on ITO/ZnO and ITO/PANI−ZnO electrodes under UV light and visible light irradiation, respectively (Figure S4, Supporting Information). The radius of the arc on the EIS Nynquist plot reflects the reaction rate occurring at the surface of the electrode.[32,33] The arc radius on the EIS Nynquist plot of all ITO/PANI−ZnO electrodes was smaller than that of the ITO/ZnO electrode, which meant a more effective separation of photogenerated electron−hole pairs and that faster interfacial charge transfer had occurred.[32,33] The smallest arc radius reflected the best photogenerated charge separation efficiency, which was obtained over the ITO/PANI−ZnO (1.0%) electrode. The action spectra, representing IPCE versus λ of the electrodes, are shown in Figure 7. The IPCE values were calculated by normalizing the photocurrent values for incident light energy and intensity.[34,35] The photocurrent action spectra of ITO/ZnO and ITO/PANI−ZnO electrodes exhibited similar photoresponses in the test region, and an important feature was that all of the ITO/PANI−ZnO electrodes showed a remarkably improved IPCE compared to that for the ITO/ZnO electrode. The maximum IPCE value of 9.13% was observed on the ITO/PANI−ZnO (1.0%) electrode, which was about 3.7-fold larger than that of the ITO/ZnO electrode (2.45%). This further confirmed that a more effective charge-separation and transfer process had occurred after ZnO was hybridized by PANI molecules. The photoelectrochemical tests were well matched with the photocatalytic experiments. According to the photocurrent graphs, EIS, and IPCE, it was indicated that ZnO hybridized by PANI caused an improvement in separation efficiency and a reduction in the recombination of photogenerated electron−hole pairs.

3.5. Mechanism for Ultraviolet Photoactivity and Photocorrosion Inhibition. It is important to detect the main oxidant in the photocatalytic process for investigating the photocatalytic mechanism.[23,25] Detection of the main oxidant could be carried out through radical and hole trapping experiments by using EDTA-2Na (hole scavenger) or *t*BuOH (radical scavenger),

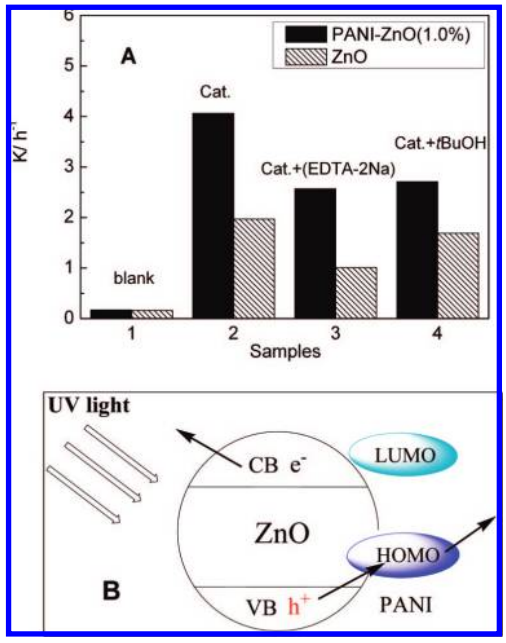

Figure 8. (A) Plots of photogenerated carrier trapping in the system of MB photodegradation over ZnO and PANI−ZnO (1.0%), respectively, with EDTA-2Na and *t*BuOH (10^{-3} M). (B) Schematic diagram illustrating the mechanism of charge separation and photocatalytic activity over PANI−ZnO photocatalysts under ultraviolet light.

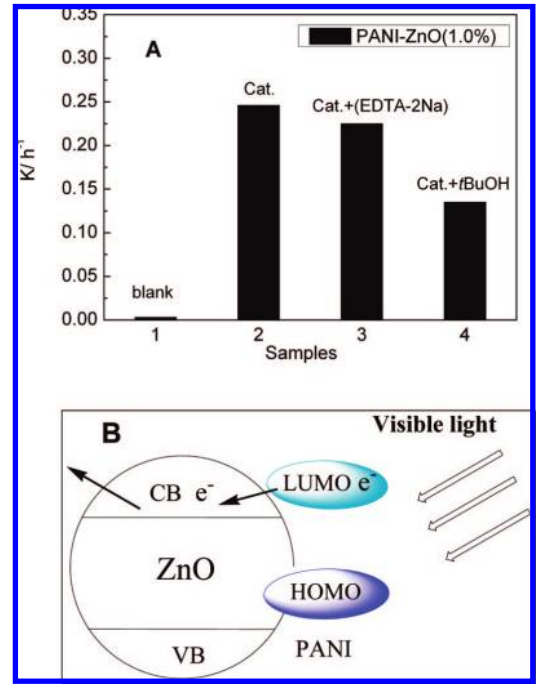

Figure 9. (A) Plots of photogenerated carrier trapping in the system of MB photodegradation over PANI−ZnO (1.0%), with EDTA-2Na and *t*BuOH (10^{-3} M). (B) Schematic diagram illustrating the mechanism of charge separation and photocatalytic activity over PANI−ZnO photocatalysts under visible light.

respectively.[36,37] As shown in Figure 8A, in the system containing ZnO photocatalysts, under UV light irradiation ZnO was induced to generate electron−hole pairs, yielding radical and hole oxidants. It revealed that the photodegradation activity of MB was supressed when either *t*BuOH or EDTA-2Na was added. Moreover, it could be seen that the photodegradation process was decelerated distinctively after EDTA-2Na was added and that the photodegradation rate was greatly decreased by about 48%. This indicated that photogenerated holes were the main oxidant and that the photocorrosion caused by holes was the dominant photocorrosion on ZnO nanocrystals.[38] As for the system of PANI−ZnO photocatalysts, the photodegradation of MB was obviously restrained after the injection of *t*BuOH or EDTA-2Na, revealing almost the same degree of decrease. This suggested that both radicals and holes were the main active species in this system. ZnO can be excited by ultraviolet light and produces photogenerated electron−hole pairs, showing photocatalytic activity. Theoretically, PANI can be excited both by UV and visible light,[27,28] but it revealed no photocatalytic activity according to the front photocatalytic experiments. The enhancement of UV light photocatalytic activity was mainly due to the high efficiency of charge separation induced by the hybrid effect of PANI and ZnO. On the basis of the results of photocatalytic and photogenerated carrier trapping tests, the schematic mechanism of charge separation and photocatalytic reaction over the PANI−ZnO photocatalyst is shown in Figure 8B. The valence band (VB) position of ZnO was lower than the HOMO of PANI, so the later could act as an acceptor for the photogenerated holes in the hybrid photocatalysts. When ZnO absorbed UV light to generate electron−hole pairs, the holes in VB could directly transfer to the HOMO of PANI.[25,39] Furthermore, PANI was a good material for transporting holes:[28,29] the holes transferred easily to the surface and oxidized the adsorbed contaminations directly.[40] Electrons moved in the opposite direction from holes, reducing the recombination of photogenerated electrons and holes and making charge separation more efficient; then the recombination of electrons and holes in PANI−ZnO was greatly suppressed, leading to a higher photocatalytic activity. Concurrently, photogenerated holes rapidly transferring to the solution successfully facilitated the inhibition of photocorrosion.

3.6. Mechanism on Visible Photoactivity. It is well known that ZnO itself is not excited by visible light. The surface hybridization with PANI will induce the visible light photon absorption. Only the influences of MB photodegradation by scavengers over PANI−ZnO photocatalysts were discussed, as shown in Figure 9A. It could be seen that the photodegradation rate changed indistinctively, decreasing by only 7.7% after the addition of EDTA-2Na. Whereas the photodegradation rate was intensively suppressed, it decreased by 45.2% when *t*BuOH was added, indicating that radicals were the main oxidant and that pollutants were eliminated mainly by means of oxygenous radical oxidation under visible light irradiation. On the basis of the results of photocatalytic and photogenerated carrier trapping tests, a schematic mechanism of the charge separation and photocatalytic reaction over the PANI−ZnO photocatalyst is shown in Figure 9B. The conduction band (CB) position of ZnO was lower than the LUMO of PANI, so the former could act as a sink for the photogenerated electrons in the hybrid photocatalysts. The PANI layer absorbed visible light to induce excited-state electrons, and the photoexcited electrons could be readily injected into the CB of ZnO and subsequently transferred to the photocatalyst surface to react with water and oxygen. This reaction yielded hydroxyl and superoxide radicals that were able to oxidize the pollutants because of their high oxidative capacity, producing visible light photocatalytic activity.

4. Conclusions

It has been demonstrated that PANI-hybridized ZnO photocatalysts possess both significant visible light oxidation activity and excellent antiphotocorrosion stability. The present hybrid photocatalysts are promising photocatalytic and photoelectric

conversion materials with good potential applications for environmental purification and hydrogen production by sufficiently utilizing solar energy. Thus, on the basis of our fundamental materials characterization a new paradigm for designing visible-light-driven, highly active, highly stable photocatalysts is being suggested.

Acknowledgment. This study was financially supported in part by the Chinese National Science Foundation (20673065) and the National Basic Research Program of China (2007CB613303).

Supporting Information Available: XRD patterns, diffuse reflectance spectra, TEM images before and after photocatalytic recycle reactions, and EIS Nynquist plots. This material is available free of charge via the Internet at http://pubs.acs.org.

References and Notes

(1) Hoffmann, M. R.; Martin, S. T.; Choi, W. Y.; Bahnemann, D. W. *Chem. Rev.* **1995**, *95*, 69–96.
(2) Matsuoka, M.; Kitano, M.; Takeuchi, M.; Tsujimaru, K.; Anpo, M.; Thomas, J. M. *Catal. Today* **2007**, *122*, 51–61.
(3) Kudo, A. *Int. J. Hydrogen Energy* **2007**, *32*, 2673–2678.
(4) Fujishima, A.; Zhang, X. T.; Tryk, A. D. *Int. J. Hydrogen Energy* **2007**, *32*, 2664–2672.
(5) Linsebigler, A. L.; Lu, G.; Yates, J. T., Jr. *Chem. Rev.* **1995**, *95*, 735–758.
(6) Chen, X.; Mao, S. S. *Chem. Rev.* **2007**, *107*, 2891–2959.
(7) Yeber, M. C.; Rodríguez, J.; Freer, J.; Durán, N.; Mansilla, H. D. *Chemosphere* **2000**, *4141*, 1193–1197.
(8) Khodja, A. A.; Sehili, T.; Pilichowski, J-T.; Boule, P. *J. Photochem. Photobiol., A* **2001**, *41*, 231–239.
(9) Ye, C.; Bando, Y.; Shen, G.; Golberg, D. *J. Phys. Chem. B* **2006**, *110*, 15146–15151.
(10) Cao, B.; Cai, W. J. *J. Phys. Chem. C* **2008**, *112*, 680–685.
(11) Fox, M. A.; Dulay, M. T. *Chem. Rev.* **1993**, *93*, 341–357.
(12) De Jongh, P. E.; Meulenkamp, E. A.; Vanmaekelbergh, D.; Kelly, J. J. *J. Phys. Chem. B* **2000**, *104*, 7686–7693.
(13) Bandara, J.; Tennakone, K.; Jayatilaka, P. P. B. *Chemosphere* **2002**, *49*, 439–445.
(14) Stroyuk, A. L.; Shvalagin, V. V.; Kuchmii, S. Ya. *Theor. Exp. Chem.* **2004**, *40*, 98–104.
(15) Jing, L. Q.; Wang, B. Q.; Xin, B. F.; Li, S. D.; Shi, K. Y.; Cai, W. M.; Fu, H. G. *J. Solid State Chem.* **2004**, *177*, 4221–4227.
(16) Lu, W. W.; Gao, S. Y.; Wang, J. J. *J. Phys. Chem. C* **2008**, *112*, 16792–16800.
(17) Qiu, X. Q.; Li, G. S.; Sun, X. F.; Li, L. P.; Fu, X. Z. *Nanotechnology* **2008**, *19*, 1–8.
(18) Qiu, X. Q.; Li, L. P.; Zheng, J.; Liu, J. J.; Sun, X. F.; Li, G. S. *J. Phys. Chem. C* **2008**, *112*, 12242–12248.
(19) Zhang, M. L.; An, T. C.; Hu, X. H.; Wang, C.; Sheng, G. Y.; Fu, J. M. *Appl. Catal., A* **2004**, *260*, 215–222.
(20) Mane, R. S.; Lee, W. J.; Pathan, H. M.; Han, S. H. *J. Phys. Chem. B* **2005**, *109*, 24254–24259.
(21) Lahiri, J.; Batzill, M. *J. Phys. Chem. C* **2008**, *112*, 4304–4307.
(22) Yu, G.; Gao, J.; Hummelen, J. C.; Wudl, F.; Heeger, A. J. *Science* **1995**, *270*, 1789–1791.
(23) Zhu, S. B.; Xu, T. G.; Fu, H. B.; Zhao, J. C.; Zhu, Y. F. *Environ. Sci. Technol.* **2007**, *41*, 6234–6239.
(24) Zhang, L. W.; Fu, H. B.; Zhu, Y. F. *Adv. Funct. Mater.* **2008**, *18*, 2180–2189.
(25) Zhang, H.; Zong, R. L.; Zhao, J. C.; Zhu, Y. F. *Environ. Sci. Technol.* **2008**, *42*, 3803–3807.
(26) Fu, H. B.; Xu, T. G.; Zhu, S. B.; Zhu, Y. F. *Environ. Sci. Technol.* **2008**, *42*, 8064–8069.
(27) Gospodinova, N.; Terlemezyan, L. *Prog. Polym. Sci.* **1998**, *23*, 1443–1484.
(28) Kang, E. T.; Neoh, K. G.; Tan, K. L. *Prog. Polym. Sci.* **1998**, *23*, 277–324.
(29) Shirota, Y.; Kageyama, H. *Chem. Rev.* **2007**, *107*, 953–101.
(30) Li, X. W.; Wang, G. C.; Li, X. X.; Lu, D. M. *Appl. Surf. Sci.* **2004**, *229*, 395–401.
(31) Xi, Y. Y.; Zhou, J. Z.; Guo, H. C.; Cai, C. D.; Lin, Z. H. *Chem. Phys. Lett.* **2005**, *412*, 60–64.
(32) Liu, H.; Cheng, S. A.; Wu, M.; Wu, H. J.; Zhang, J. Q.; Li, W. Z.; Cao, C. N. *J. Phys. Chem. A* **2000**, *104*, 7016–7020.
(33) Leng, W. H.; Zhang, Z.; Zhang, J. Q.; Cao, C. N. *J. Phys. Chem. B* **2005**, *109*, 15008–15023.
(34) Hasobe, T.; Imahori, H.; Fukuzumi, S.; Kamat, P. V. *J. Phys. Chem. B* **2003**, *107*, 12105–12112.
(35) Hasobe, T.; Murata, H.; Kamat, P. V. *J. Phys. Chem. C* **2007**, *111*, 16626–16634.
(36) Minero, C.; Mariella, G.; Maurino, V.; Vione, D.; Pelizzetti, E. *Langmuir* **2000**, *16*, 8964–8972.
(37) Xu, T.; Cai, Y.; O'Shea, K. E. *Environ. Sci. Technol.* **2007**, *41*, 5471–5477.
(38) Kamat, P. V.; Dimitrijevic, N. M.; Fessenden, R. W. *J. Phys. Chem.* **1987**, *91*, 396–401.
(39) Li, J.; Zhu, L. H.; Wu, Y. H.; Harima, Y.; Zhang, A. Q.; Tang, H. Q. *Polymer* **2006**, *47*, 7361–7367.
(40) Carrway, E R.; Hoffman, A. J.; Hoffmann, M. R. *Environ. Sci. Technol.* **1994**, *28*, 786–79.

JP810748U